IET Inspec

Inspec Analytics

# Uncover deeper insights into the impact of global research

Understand your place in the global engineering research landscape and make strategic decisions about the direction of your projects with a dynamic research intelligence tool based on the IET's renowned Inspec database.

## Precision analytics for research excellence

Enhanced features allow you to uncover deeper insights into the impact of global research and explore the elements most valuable to you. With Inspec Analytics, you can:

- Deepen your understanding of global scientific trends.
- Define the scope of research initiatives to maximise your impact.
- Assess your organisation's research output and impact.
- Evaluate the success of collaborative partnerships.

Learn more at **inspec-analytics.theiet.org**

IET Power Electronics

Research Article

# Robust feedback-linearisation control of a boost converter feeding a grid-tied inverter for PV applications

ISSN 1755-4535
Received on 31st January 2017
Revised 17th September 2017
Accepted on 12th November 2017
doi: 10.1049/iet-pel.2017.0084
www.ietdl.org

*Rachid Errouissi*[1], *Ahmed Al-Durra*[1] ✉, *S.M. Muyeen*[2], *Abdelali El Aroudi*[3]
[1]*Electrical and Computer Engineering, Khalifa University of Science and Technology, Abu Dhabi, United Arab Emirates*
[2]*Department of Electrical and Computer Engineering, Curtin University, Perth, Australia*
[3]*Departament d'Enginyeria Electrónica, Elètrica i Automàtica, Escola Tècnica Superior d'Enginyeria, Universitat Rovira i Virgili, 43007 Tarragona, Spain*
✉ *E-mail: aaldurra@pi.ac.ae*

**Abstract:** In this study, the feedback-linearisation (FBL) technique is employed to design a dc–dc boost voltage regulator feeding a grid-tied inverter for photovoltaic (PV) systems. The key feature of the proposed approach is that only a voltage control loop is used to generate the driving signal for the converter and no current control loop is required. Thereby, unlike the cascaded structure, the bandwidth of the voltage control loop can be specified only by the switching frequency as there is no need for an intermediate inner-loop. The major concern of this control scheme is its limited ability to eliminate completely the steady-state error under model uncertainty and unknown disturbance such as the PV current, which is considered as an unmatched disturbance. For this purpose, the unknown perturbation is estimated by a disturbance observer and compensated in the control law to drive the steady-state error to zero. With a fast disturbance estimation, the composite controller is able to retain the nominal transient performance specified with the FBL. The effectiveness of the proposed approach was verified by both simulation and experimental results, and a remarkable agreement was obtained while exhibiting excellent performances.

## 1 Introduction

Several topologies have been developed to ensure sustainable, reliable and efficient use of solar energy in either grid-connected or stand-alone photovoltaic (PV) applications [1]. For a grid-connected operation, either single or dual-stage inverter can be used in PV applications. The single-stage PV inverter is attractive and offers numerous advantages depending on the power converter topology [2–5]. A typical topology of the dual-stage inverter consists of a dc–dc boost converter and a dc–ac inverter, as shown in Fig. 1. Compared with the dual-stage inverter, the single-stage inverter has the advantage of less switching devices, since only a single-stage power conversion is required. The main advantage of the dual-stage inverter, in comparison with the single-stage inverter, is its ability to achieve a tight regulation of the dc-link voltage through the control of the dc–ac inverter. Relying on the assumption that the dc-link voltage is tightly regulated, maximum power point tracking (MPPT) operation can easily be performed through the control of the dc–dc boost converter [6–8]. This partly explains why the dual-stage inverter is widely used in PV applications. The MPPT algorithms generate a reference which can be used for either direct duty-cycle control, PV voltage control or current control of the dc–dc boost converter. However, it is wise to regulate the PV voltage as it changes slowly with the atmospheric conditions. Cascaded structure consisting of an outer voltage regulator and an inner current controller is widely adopted for applying MPPT algorithms. For the inner loop, several control techniques have been proposed to control the inductor current $i_L$ including model predictive control (MPC) [9], sliding mode control [10, 11], proportional–integral (PI) regulator [12] and so on.

For the outer loop design, the methodology for controlling the PV voltage $v_0$ is mainly based on the approximate $i_L$-to-$v_o$ transfer function $1/C_b s$. Such a transfer function cannot exactly represent the transient behaviour of the system model, particularly when the input capacitor $C_b$ is relatively small due to the neglect of the dynamic resistance $R_{\text{pv}}$ [13]. Another issue is that the dynamic resistance is highly dependent on the characteristic of the PV array and varies with the atmospheric conditions and the operating points as $R_{\text{pv}} = -\partial v_0/\partial i_p$. The concerns regarding the influence of the dynamic resistance on the control performance were addressed in several research works [13–17]. Indeed, a relatively large capacitance of the input capacitor cancels the effect of the dynamic resistance, and a simple PI is able to achieve stability and good dynamic performances under different operating points. In other words, under a large value of $C_b$, the current to voltage transfer function can be approximated with $1/C_b s$ despite the variation of the dynamic resistance. In such a case, a robust PI regulator can be designed using only the current to voltage transfer function $1/C_b s$

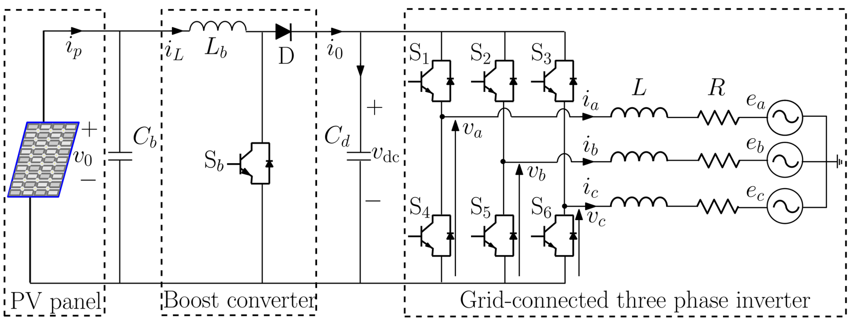


**Fig. 1** *Schematic diagram of a grid-connected PV inverter system*

without considering the variability of $R_{\mathrm{pv}}$. However, with a relatively small input capacitor, the use of a conventional PI controller for the PV voltage regulation may not be the right choice as the resulting bandwidth of the closed-loop system changes with the variation of the operating points due to the effect of $R_{\mathrm{pv}}$. Hence, an adequate method to overcome such a drawback is to consider the variation of the dynamic resistance in the control design in order to compensate for its effect regardless of the input capacitance value.

In recent years, several techniques have been proposed to develop suitable controllers taking into account the dynamic resistance variations. In [13], the dynamic resistance is estimated and its value is used to update the parameters of the controller. The resulting controller provided satisfactory results with preservation of the desired transient performance under different operating points. However, a precise knowledge of the input capacitor is required to achieve accurate compensation of the dynamic resistance, which raises concerns about robustness. This reveals the need for other techniques that are more robust against all uncertainties. A robust digital control is presented in [17] using Youla parametrisation, where the voltage regulator generates directly the required duty cycle for the pulse width modulation (PWM) scheme associated with the controller. In this paper, an alternative approach is proposed to control a dc–dc boost converter feeding a grid-tied inverter for PV applications. In the proposed control scheme, the duty cycle is directly determined by the voltage regulation without the need for a current controller, and the dynamic resistance is not considered in the controller design. Instead, the PV array is considered as an unknown current source, which is estimated and then compensated by the controller. The method proposed in this work is based on combining a feedback-linearisation (FBL) technique with a disturbance observer (DO) to compensate for model uncertainty and unknown perturbation [18]. Specifically, a DO-based control (DOBC) [19] is adopted to estimate both matched and unmatched disturbances resulting from parameter variation and unknown PV current $i_p$. The DOBC used in this work is a kind of high-gain observer technique. This implies that, with a fast DOBC, the composite controller can recover the nominal transient performance specified with the FBL [18]. Such a promising feature is guaranteed under the utilisation of high observer gain. In recent years, several research works [20–22] have shown that combining a DO with a baseline controller is the most effective way to improve both the transient and the steady-state performances of power converters. The only attempt to apply a DO technique to a boost converter interfaced with PV generators was recently proposed in [21, 22]. In both works, a two-loop cascaded approach was used. In [21], the DO has been combined with a convectional PI controller to preserve the nominal tracking performance over the entire operating range in a stand-alone operation and without an experimental validation. In [22], DO is combined with MPC to synthesise a PI controller for a dc–dc boost converter. Such a control scheme allows having a better transient performance compared with a conventional PI controller, but its bandwidth is constrained by the use of the cascaded structure. In other words, the voltage control loop should be designed to have a relatively slow dynamic response in comparison with the inner loop.

The main objective of this work is to practically apply FBL technique together with DOBC to a dc–dc boost converter feeding a grid-connected inverter. The idea is to explore the nominal performance recovery property of the composite controller, aiming to provide good transient and steady-state performances for the whole operating range despite the presence of model uncertainty and unknown disturbance. Also, a good dynamic response can be achieved under control input saturation without additional compensator [23]. Another promising feature of the composite controller is that the estimation of the PV current $i_p$ can be directly used in MPPT algorithm instead of the current measurement.

## 2 Modelling of the dc–dc boost converter

As shown above in Fig. 1, the complete PV system consists of a dc–dc boost converter, a dc-link capacitor $C_d$ and a three-phase inverter connected to the grid via an $L$ line filter. The major role of the boost converter is to control the PV voltage $v_0$ to extract the maximum power available from the PV system. For the boost converter, the dc-link voltage $v_{\mathrm{dc}}$ is viewed as an input, which is maintained constant with an appropriate control of the three-phase grid-connected inverter. The main focus of this study is the control of a dc–dc boost converter by adjusting the duty cycle of the driving signal applied to its switch $S_b$. Under continuous conduction mode (CCM), the dynamics of the boost converter are governed by the following set of differential equations:

$$\begin{cases} \dfrac{\mathrm{d}i_L}{\mathrm{d}t} = \dfrac{v_0}{L_b} - \dfrac{v_{\mathrm{dc}}}{L_b} + \dfrac{v_{\mathrm{dc}}}{L_b}u \\ \dfrac{\mathrm{d}v_0}{\mathrm{d}t} = -\dfrac{i_L}{C_b} + \dfrac{i_p}{C_b} \end{cases} \tag{1}$$

where $i_L$ is the current of the inductor and $v_0$ is the voltage of the capacitor $C_b$ which coincides with the voltage at the output of the PV generator. $C_b$, $L_b$, $i_p$ and $u$ represent, respectively, the capacitance of the input capacitor, the inductance of the boost inductor, the PV current and the duty-cycle control. It is worth noticing that a precise knowledge of the model is not possible. Moreover, the information about the PV current is not always available for measurement and it depends on the changes in atmospheric conditions. Therefore, to consider the system variability and the model uncertainties, the set of differential equations in (1) can be rewritten as follows:

$$\begin{cases} \dfrac{\mathrm{d}i_L}{\mathrm{d}t} = \dfrac{v_0}{L_b} - \dfrac{v_{\mathrm{dc}}}{L_b} + \dfrac{v_{\mathrm{dc}}}{L_b}u + \dfrac{b_1}{L_b} \\ \dfrac{\mathrm{d}v_0}{\mathrm{d}t} = -\dfrac{i_L}{C_b} + \dfrac{b_2}{C_b} \end{cases} \tag{2}$$

In (2), uncertainties $b_1$ and $b_2$ represent the additive lumped disturbances that can affect the closed-loop system performances, and they include the PV current $i_p$, unknown disturbance and model uncertainty. Here, it is assumed that the measurements are accurate, meaning that the sensor gains do not include disturbances. Let $\boldsymbol{x}$ be the vector of state variables, $\boldsymbol{b}$ be the vector of matched and unmatched disturbances and $y$ is the output that can be expressed as follows:

$$\boldsymbol{x} = [i_L \quad v_0]^{\mathrm{T}}, \quad \boldsymbol{b} = [b_1 \quad b_2]^{\mathrm{T}}, \quad y = v_0 \tag{3}$$

In (2), the dc-link voltage $v_{\mathrm{dc}}$ is assumed to be tightly regulated. Hence, the perturbed model (2) can be rewritten in the linear form as follows:

$$\begin{cases} \dot{x} = \boldsymbol{A}\boldsymbol{x} + \boldsymbol{B}_u(u-1) + \boldsymbol{B}_b\boldsymbol{b} \\ y = \boldsymbol{C}\boldsymbol{x} = [0 \quad 1]\boldsymbol{x} \end{cases} \tag{4}$$

where the matrices $\boldsymbol{A}$, $\boldsymbol{B}_u$ and $\boldsymbol{B}_b$ are given by

$$\boldsymbol{A} = \begin{bmatrix} 0 & \dfrac{1}{L_b} \\ -\dfrac{1}{C_b} & 0 \end{bmatrix}, \quad \boldsymbol{B}_u = \begin{bmatrix} \dfrac{v_{dc}}{L_b} \\ 0 \end{bmatrix}, \quad \boldsymbol{B}_b = \begin{bmatrix} \dfrac{1}{L_b} & 0 \\ 0 & \dfrac{1}{C_b} \end{bmatrix} \tag{5}$$

Clearly, $b_1$ represents a matched disturbance whereas $b_2$ is considered as an unmatched one for the given input. It is noticed that in the absence of model uncertainties, the disturbance $b_2$ only represents the PV current $i_p$, which becomes equal to the inductor current $i_L$ in the steady-state regime.

*Assumption:* The disturbance $\boldsymbol{b}$ is assumed to be bounded and satisfies

$$\lim_{t \to \infty} \dot{b} = 0 \tag{6}$$

which is a reasonable assumption as the PV current is mainly decided by the operating point.

## 3 FBL control for the boost converter

### 3.1 Formulation of the control law

In the FBL technique presented in [24], the relative degree of the system is required to design a state feedback control law. For the system under study, the relative degree is $\rho = 2$. Let the Markov parameters $m_{uk} = CA^k\boldsymbol{B}_u$ and $m_{bk} = CA^k\boldsymbol{B}_b$, $k = 0, 1, 2, \ldots$ corresponding to control-to-output and disturbance-to-output system transfer functions. Then, by differentiating the tracking error $e(t) = y_{\text{ref}} - y$, with $y_{\text{ref}}$ is the reference of the PV voltage, it can be shown that

$$\begin{cases} \dot{e}(t) = \dot{y}_{\text{ref}}(t) - \boldsymbol{CAx} - m_{b0}\boldsymbol{b} \\ \ddot{e}(t) = \ddot{y}_{\text{ref}}(t) - \boldsymbol{CA}^2\boldsymbol{x} - m_{u1}\overline{u} - m_{b1}\boldsymbol{b} - m_{b0}\dot{b} \end{cases} \tag{7}$$

where $\overline{u} = 1 - u$.

Following [24], a state feedback control $\overline{u}$ is given by

$$\overline{u} = 1 - u = \frac{\Gamma(x) - (K_1 m_{b0} + m_{b1})\boldsymbol{b} - m_{b0}\dot{b}}{m_{u1}} \tag{8}$$

where $\Gamma(x)$ is given by the following expression:

$$\Gamma(x) = K_0 e(t) + K_1(\dot{y}_{\text{ref}} - \boldsymbol{CAx}) + \left(\ddot{y}_{\text{ref}} - \boldsymbol{CA}^2\boldsymbol{x}\right) \tag{9}$$

Here, it is clear that the control input $\overline{u}$ will exist whenever $m_{u1} := \boldsymbol{CAB}_u \neq 0$, i.e. $v_{\text{dc}} \neq 0$. The controller gains $K_0$ and $K_1$ can be selected based on the performance specifications. Specifically, the controller gains should be chosen such that the polynomially $P(s)$ given below is Hurwitz

$$P(s) = s^2 + K_1 s + K_0 \tag{10}$$

Realising that, with assumption (6), the term $\dot{b}$ will disappear from the control law (8) in the steady-state regime. Thus, for a real-time implementation, $\dot{b}$ can be neglected in the control law, yielding

$$\overline{u} = \frac{\Gamma(x) - (K_1 m_{b0} + m_{b1})\boldsymbol{b}}{m_{u1}} \tag{11}$$

Substituting (11) in (7) gives the differential equation governing the error dynamics which can be written in the following form:

$$\ddot{e}(t) = -K_1\dot{e}(t) - K_0 e(t) + m_{b0}\dot{b} \tag{12}$$

With the fact that the disturbance $\dot{b}$ is bounded, and the polynomial $P(s)$, given in (10), is Hurwitz, it is clear that the closed-loop system is stable. In other words, the system (12) is input-to-state stable with respect to the disturbance input $\dot{b}$ [24]. According to [25], the bounded tracking error $e(t)$ can be made smaller by choosing the controller gains as follows:

$$K_0 = \frac{\alpha_0}{\tau^2}, \quad K_1 = \frac{\alpha_1}{\tau} \tag{13}$$

where $\tau$ is a small positive parameter, and $\alpha_{\{0,1\}}$ are any chosen parameters such that the following polynomial $P_\alpha(s)$:

$$P_\alpha(s) = s^2 + \alpha_1 s + \alpha_0 \tag{14}$$

is Hurwitz.

Let $\alpha_{\{0,1\}} = 2$, and assuming that the disturbance $\boldsymbol{b}$ is generated by a constant signal, i.e. $\dot{b} = 0$; therefore, from (12), it follows that the reference-to-output transfer function is basically a typical second-order system whose characteristic polynomial is given by

$$\sigma(s) = s^2 + 2\xi\omega_n s + \omega_n^2 \tag{15}$$

where $\omega_n = \sqrt{K_0}$ is the natural angular frequency and $\xi = K_1/2\sqrt{K_0}$ is the damping factor. Invoking (13), it can be verified that

$$\omega_n = \sqrt{2}\tau^{-1}, \quad \xi = 0.707 \tag{16}$$

which implies that $t_s \simeq 4/\zeta\omega_n = 4\tau$, where $t_s$ is the closed-loop settling time, hence, the parameter $\tau$ is the equivalent time constant of the closed-loop system.

*Remark 1:* For the system under study, the term $\dot{b}$ varies with time, and $\lim_{t\to\infty} \dot{b} = 0$, indicating that the system output will track its reference with an error that vanishes as $t \to \infty$ provided that the closed-loop system is stable.

*Remark 2:* When $\tau$ is sufficiently small, the feedback controller acts as a high-gain feedback control, described in [26]. Thereby, a smaller $\tau$ implies a faster response and a smaller steady-state error in the presence of unknown disturbance not considered in the control design. From a practical standpoint, decreasing $\tau$ to increase the gain of the controller will eventually magnify the measurement noise. On the other hand, as the term $\dot{b}$ vanishes only in the steady-state regime, it is clear that the real closed-loop settling time will be eventually different from the specified one, defined as $4\tau$. Thereby, the parameter $\tau$ should be chosen as small as feasible, with the consideration of the practical limitations and the value of the switching frequency $f_{\text{sw}}$ that constraints the minimum value of the settling time as $\min(t_s) = 8 \sim 10/f_{\text{sw}}$, with $f_{\text{sw}}$ is the switching frequency [9, 11, 27].

The information about the disturbance $\boldsymbol{b}$ is required to practically implement the control law (11). To address such a requirement, both matched and unmatched disturbances are estimated and compensated in the control law by designing a DO based on the plant model.

### 3.2 Disturbance observer

The previous proposed controller was derived by assuming that both, inductor current $i_L$ and capacitor voltage $v_0$, are available for direct measurement. Hence, as all states are measurable, a DO can be designed and combined with the control law to achieve a zero static error for the system. As in [19], a DO can be expressed as follows:

$$\dot{\hat{b}} = -\mu\boldsymbol{B}_b\hat{b} + \mu(\dot{x} - \boldsymbol{Ax} - \boldsymbol{B}_u(u_{\text{eff}} - 1)) \tag{17}$$

where $u_{\text{eff}}$ is the effective duty cycle, and is given by

$$u_{\text{eff}} = \text{sat}(u) = \begin{cases} 0, & u < 0 \\ u, & u \in [0, 1] \\ 1, & u > 1 \end{cases} \tag{18}$$

and $\boldsymbol{\mu}$ is the observer gain matrix and it can be chosen as

$$\boldsymbol{\mu} = \frac{\partial D}{\partial x} \tag{19}$$

For the system under study, the matrix $\boldsymbol{D}$ is given by

$$\boldsymbol{D} = \begin{bmatrix} \mu_1 i_L & \mu_2 v_0 \end{bmatrix}^{\mathrm{T}} \to \boldsymbol{D} = \boldsymbol{\mu x} \tag{20}$$

Thus, the observer gain matrix $\boldsymbol{\mu}$ can be reduced to

$$\boldsymbol{\mu} = \begin{bmatrix} \mu_1 & 0 \\ 0 & \mu_2 \end{bmatrix} \tag{21}$$

From (3) and (17), it follows that the disturbance estimation error $e_b = \hat{b} - \boldsymbol{b}$ is governed by

$$\dot{e}_b = -\boldsymbol{\mu}\boldsymbol{B}_b e_b - \dot{b} \tag{22}$$

Therefore, with assumption (6), the asymptotic stability of the DO can be guaranteed by an appropriate choice of the observer gain matrix $\boldsymbol{\mu}$. More specifically, by considering the structure of $\boldsymbol{B}_b$, it is clear that the DO can be made stable by choosing $\mu_{1,2} > 0$, which makes the matrix $-\boldsymbol{\mu}\boldsymbol{B}_b$ Hurwitz. Moreover, as $\lim_{t\to\infty}\dot{b} = 0$ the disturbance estimation error converges to zero in the steady-state regime, implying the asymptotic stability of the DO. It is noticed that the rate of convergence for the DO is highly dependent on the observer gain. Indeed, a large value of $\mu_{1,2}$ leads to a fast disturbance estimation and enables to preserve the nominal tracking performance [28]. The main concern about the proposed DO is that the time derivative of the state is required for real-time implementation, which is not always available. Such a drawback can be overcome by modifying the proposed DO as follows:

$$\begin{cases} \dot{\hat{z}} = -\boldsymbol{\mu}\boldsymbol{B}_b(\hat{z} + \boldsymbol{\mu}\boldsymbol{x}) - \boldsymbol{\mu}(\boldsymbol{A}\boldsymbol{x} + \boldsymbol{B}_u(u_{\text{eff}} - 1)) \\ \hat{b} = \hat{z} + \boldsymbol{\mu}\boldsymbol{x} \end{cases} \tag{23}$$

where $z$ is an auxiliary state to be estimated based on the plant model and the state measurement, with $\hat{z}(0) = -\boldsymbol{\mu}\boldsymbol{x}(0)$. The DO (23) is basically a reduced-order high-gain observer [29]. Therefore, increasing the observer gain makes the closed-loop response, under the composite controller, to asymptotically approach the one achieved with the state feedback control (11). Such a feature can be achieved at the expense of the magnification of the measurement noises because of the derivative of the output [30]. Thus, a tradeoff between a fast disturbance rejection and measurement noises attenuation should be made when selecting the observer gain to prevent magnifying the voltage/current fluctuations.

### 3.3 Overall closed-loop stability

First, note that the effective controller is given by

$$\bar{u} = \frac{\Gamma(x) - (K_1 m_{b0} + m_{b1})\hat{b}}{m_{u1}} \tag{24}$$

The closed-loop stability of the composite controller can be analysed by investigating the stability of the closed-loop error dynamics. Indeed, substituting the control law (24) in (7) yields

$$\ddot{e} = -K_1\dot{e} - K_0 e + (K_1 m_{b0} + m_{b1})e_b + m_{b0}\dot{b} \tag{25}$$

Let $\eta = [e \quad \dot{e}]^{\text{T}}$, and combining (25) with the observer error equation (22), gives the closed-loop system error equations as follows:

$$\begin{bmatrix} \dot{\eta} \\ \dot{e}_b \end{bmatrix} = \begin{bmatrix} \boldsymbol{A}_\eta & A_b \\ \boldsymbol{0}_{2\times 2} & -\boldsymbol{\mu}B_b \end{bmatrix} \begin{bmatrix} \eta \\ e_b \end{bmatrix} + \begin{bmatrix} B_\eta \\ -\boldsymbol{I}_{2\times 2} \end{bmatrix} \dot{b} \tag{26}$$

where $\boldsymbol{I}_{2\times 2}$ and $\boldsymbol{0}_{2\times 2}$ are $2\times 2$ identity and null matrices, respectively, and

$$A_b = \begin{bmatrix} \boldsymbol{0}_{1\times 2} \\ (K_1 m_{b0} + m_{b1}) \end{bmatrix}, \quad B_\eta = \begin{bmatrix} \boldsymbol{0}_{1\times 2} \\ m_{b0} \end{bmatrix} \tag{27}$$

The matrix $\boldsymbol{A}_\eta$ is given by

$$\boldsymbol{A}_\eta = \begin{bmatrix} 0 & 1 \\ -K_0 & -K_1 \end{bmatrix} \tag{28}$$

It can easily be shown that the matrix $\boldsymbol{A}_\eta$ is Hurwitz. Thereby, as $-\boldsymbol{\mu}\boldsymbol{B}_b$ is also Hurwitz, the closed-loop system error defined by (26) is input-to-state stable with respect to the disturbance input $\dot{b}$. This means that the errors $e$ and $e_b$ are bounded and their bounds are proportional to the bound on the input $\dot{b}$ (see section 4.9 in [24]). Therefore, with the assumption that $\lim_{t\to\infty}\dot{b}(t) = 0$, one can conclude that the tracking error $e$ converges to zero as $t \to \infty$.

*Remark 3:* As pointed out above, the mathematical model of the dc–dc boost converter is derived for CCM. Therefore, no conclusion can be drawn about the feasibility of the composite controller for discontinuous conduction mode (DCM), as the design methodology mainly depends on the mathematical model of the system under study. Nevertheless, the control design framework, presented in this work, can also be adopted to investigate the efficacy of the proposed controller for DCM.

*Remark 4:* For the system under study, the control design is relatively simple, as FBL technique and DO approach are relatively conventional. On the other hand, only the mathematical tools of linear systems analysis were used to show the stability of the closed-loop system under the composite controller. This is because, under the assumption that $v_{\text{dc}}$ is tightly regulated, the mathematical model of the dc–dc boost converter becomes linear. However, as FBL technique is originally designed for non-linear systems, the control design framework, described in this work, can also be applied to other topologies of power-electronic converters that are represented by complex models. In such cases, a non-linear DO is required to ensure asymptotic stability of the closed-loop system. However, as pointed out in [31], the stability analysis of the non-linear DO itself is a challenging task, particularly when the system is subject to unmatched disturbance. Therefore, attention should be given when designing the proposed composite controller for other topologies of power-electronic converters. Nevertheless, the proposed controller can easily be applied to specific power-electronic converters that are represented by non-linear models such as grid-tied inverter [32]. Indeed, as presented in [32], when the system under study is non-linear, the mathematical tools of non-linear systems analysis can be adopted to investigate the stability of the closed-loop system under the composite controller consisting of a FBL and non-linear DO. It is important to emphasise that the composite controller was designed based on assumption (6), i.e. $\dot{b} = 0$, which is not true for several power-electronic converters. Therefore, in the future, the main research work will be focusing on adapting the proposed controller to consider wide range of disturbances, e.g. periodic perturbation, for power converters found in renewable energy conversion systems.

## 4 Computer simulations

### 4.1 Control loop diagram

Fig. 2*a* shows the block diagram for testing the composite controller consisting of the FBL (24) and the DO (23). The limitation of the duty cycle $u$ is realised through the use of a saturation block. The developed grid-connected PV system, shown in Fig. 1, was simulated using a Matlab/Simulink model. The parameters of the complete system are provided in Tables 1 and 2 of Appendix. A cascaded structure, consisting of an outer and inner loop, is employed to control the dc-link voltage and the reactive power generated to the grid. The control design for the grid-side converter is not described here, as it is beyond the scope of this work. The sampling time of the complete plant model is set equal to 1 µs, while the control period is equal to 100 µs. The switching frequency for both the boost converter and the inverter is set to be equal to 10 kHz. The single diode PV panel model, developed in [33], is considered in this work to test the proposed controller under realistic conditions. The *P–V* characteristic is shown in Fig. 2*b*, where the maximum power has been limited to 1.2 kW. Here, the dc-link voltage reference $v_{\text{dcref}}$ is fixed to 165 V, which is slightly larger than the open-circuit voltage of the PV module.

### 4.2 Comparison between the composite controller and PI controller

The simulation test was performed to compare the performance of the composite controller with that of a cascaded PI controller. The parameters $K_{pi}$ and $K_{ii}$ of the PI controller for the inner-loop are

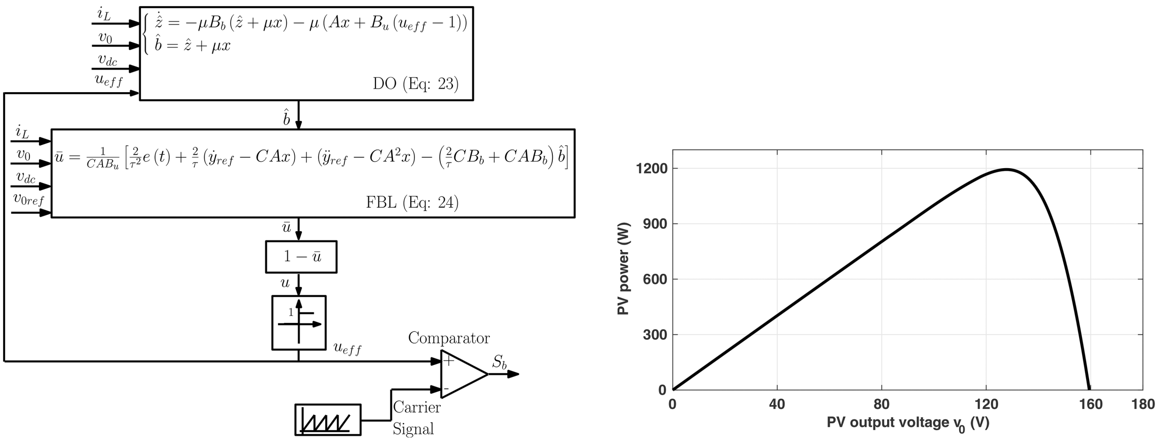


*a* *b*

**Fig. 2** *Block diagram for testing the composite controller consisting of the FBL and the DO*
***(a)*** Block diagram of the composite controller for the boost converter, ***(b)*** *P–V* characteristic of the used PV module under standard weather conditions: temperature $T = 25^{\circ}$C, and irradiance $S = 1000\,\mathrm{Wm}^{-2}$

designed as $K_{pi} = 2L_b\xi_i\omega_{ni}$ and $K_{ii} = L_b\omega_{ni}^2$, with $\xi_i$ and $\omega_{ni}$ are the damping ratio and the natural angular frequency for the current controller, respectively. The coefficient $\omega_{ni}$ can be tuned according to the performance specification of the settling time $t_{si}$ as $\omega_{ni} = 4(t_{si}\xi_i)^{-1}$. Following [9, 11, 27], the minimum settling time is dictated by the switching frequency as min $(t_{si}) = 8 \sim 10T_{sw}$, with $T_{sw} = 1/f_{sw}$ is the switching period. In this work, the settling time $t_{si}$ is set to be equal to nine times the switching period, i.e. $t_{si} = 9T_{sw}$. The coefficients $K_{pv}$ and $K_{iv}$ of the PI controller for the outer-loop are determined as $K_{pv} = 2C_b\xi_v\omega_{nv}$ and $K_{iv} = C_b\omega_{nv}^2$, with $\xi_v$ and $\omega_{nv}$ represent the damping ratio and the natural angular frequency for the outer voltage regulator, respectively. The parameter $\omega_{nv}$ can be specified as $\omega_{nv} = 4(t_{sv}\xi_v)^{-1}$, with $t_{sv}$ is the closed-loop settling time for the voltage control. To guarantee a stable control under a cascaded PI controller, the voltage control loop should be designed to have a slower response than the current loop. Moreover, to have a fair comparison the settling time $t_{sv}$ should be chosen as small as feasible; that is $t_{sv} = 9t_{si}$. Both damping ratios $\xi_i$ and $\xi_v$ are chosen equal to 0.7.

For the composite controller, the parameter $\tau$ represents the first design consideration, and it is selected to be as short as feasible with the consideration of the theoretical closed-loop settling time $t_s = 4\tau$, the minimum settling time min $(t_s) = 8 \sim 10/f_{sw}$, and the practical limitations. The second design consideration is the observer gain, which should also be chosen sufficiency small to have a fast disturbance rejection. However, as mentioned above, the measurement noises impose a practical limit on how large the observer gains could be. That is, the observer gains are chosen as $\mu_1 = 2$ and $\mu_2 = 0.1$. For purposes of performance comparison, the proposed controller was tested under three different values of $\tau$ as $\tau = \{0.00025, 0.0008, 0.001\}$. A filtered reference is used for $\tau = \{0.0008, 0.001\}$, while a step input is adopted for $\tau = 0.00025$ to saturate the control input $u$ during transients. The step response test was performed to verify the ability of the proposed controller to compensate for the effect of the saturation block. Moreover, the simulation test was conducted under two values of the input capacitor $C_b$ to highlight the effect of the input capacitance value on the control performance.

As shown in Figs. 3*a–c* and 4*a–c*, both controllers provide almost similar transient performance when the input capacitor is relatively big because of the large value of $C_bR_{pv}\omega_c$, ($\omega_c$ is the angular cutoff frequency of the voltage control loop, see Appendix), but a significant difference is observed with a small input capacitor. In particular, under a small input capacitor, the transient behaviour depends on the operating point, which can be explained by the variability of the dynamics resistance. Specifically, when the PV voltage approaches the open-circuit voltage, the dynamic resistance decreases leading to the transient performance degradation because of the small value of $C_bR_{pv}\omega_c$. However, it is clear that better transient performance can be obtained with a reduced PV voltage because of the increase of the dynamic resistance. Fig. 3*d* shows that the proposed controller needs a shorter period to leave the saturation region in comparison with the PI controller. This implies that the composite controller can also attenuate the effect of the windup phenomenon that may arise because of the integral action property of the DO. Having designed the PI controller with the minimum possible settling time, it can be said that a fair comparison was performed, and it can be concluded that the proposed controller offers better transient performance in comparison with the PI controller when the input capacitor is relatively small.

## 5 Experimental results

### *5.1 Experimental setup*

To further verify the effectiveness of the proposed controller, experimental tests were performed based on the system configuration shown in Fig. 1 and the laboratory setup depicted in Fig. 5*a*. A 2 kW Magna-Power Electronics module was used to emulate a PV array by producing a realistic *P–V* characteristic as given in Fig. 2*a*. The input capacitor $C_b$ in the experimental tests is imposed by the PV emulator as $C_b = 160\,\mu$F, and it was not possible to reduce it. The DS1103 board was employed to control both the boost converter and the grid-connected inverter. It is equipped with Power PC 750GX (Master processor) running at 1 GHz, and a Texas Instruments TMS320F240 DSP (slave processor) running at 20 MHz. For real-time implementation, the parameters of the controller are selected similar to those used for the previous test, and the only difference is the parameter $\tau$ that is selected $\tau = 0.001$ to avoid magnification of the measurement noises.

### *5.2 Tracking performance under nominal parameters*

In this experiment, the composite controller is tested under a step decrease of the PV output voltage. Indeed, at $t = 0.2$ s, the PV output voltage is suddenly stepped down from 160 to 130 V, to make the PV panel operates at MPP. It is noticed that the PV voltage reference is realised by a second-order linear filter to explore the tracking capability of the proposed controller. The composite controller is determined with the nominal parameters, and only the PV current $i_p$ is considered as an unknown disturbance. The experimental results shown in Fig. 5*b* confirm the theoretical analysis for a fast and accurate response of the PV voltage, which reaches rapidly its new steady-state value in response to a step change. However, the dynamic response of the inductor current $i_L$ is evidently slower than that of the PV voltage $v_0$ due to the inherent dynamics of the PV emulator in response to a rapid change of the PV output voltage. More importantly, the DO

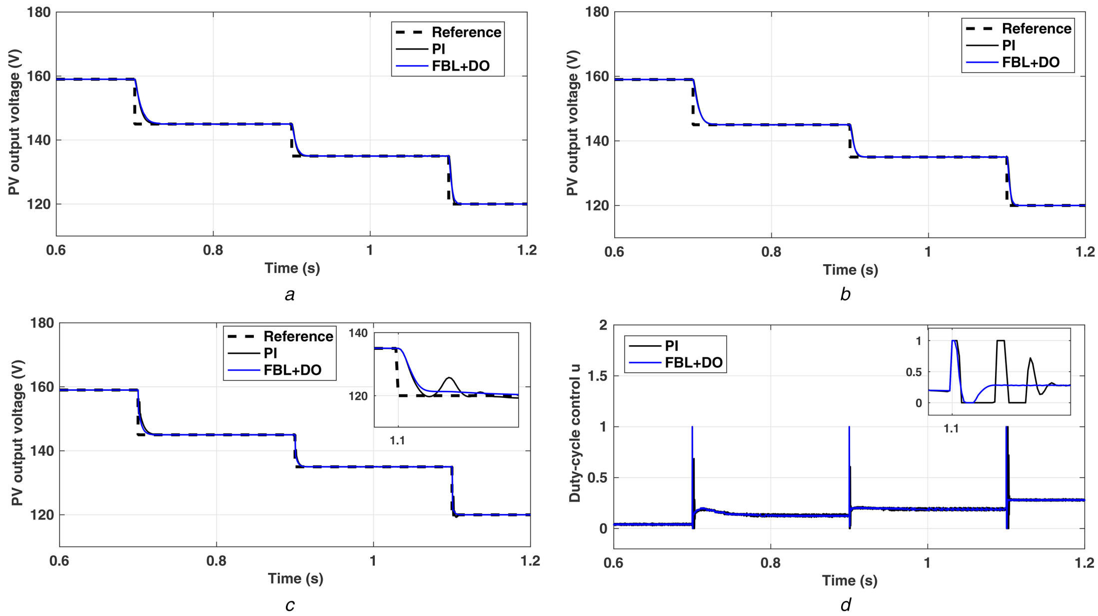


**Fig. 3** *Comparison between the proposed composite controller and the PI controller when* $C_b = 200\,\mu\text{F}$

***(a)*** Reference tracking: PV voltage response with $\tau = 0.001$, ***(b)*** Reference tracking: PV voltage response with $\tau = 0.0008$, ***(c)*** Step response: PV voltage response with $\tau = 0.00025$, ***(d)*** Step response: duty cycle with $\tau = 0.00025$

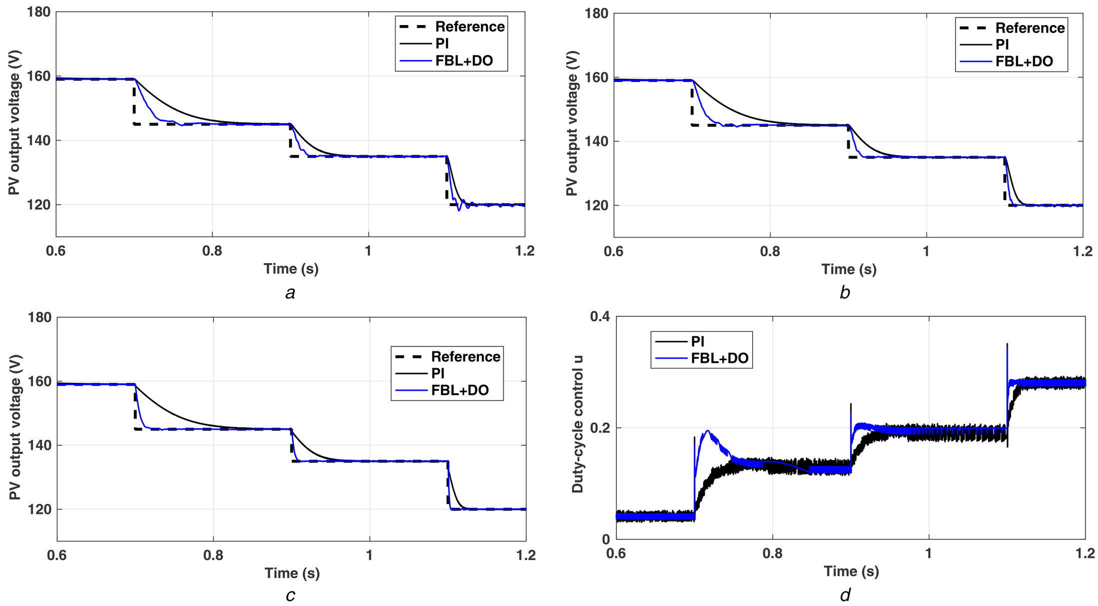


**Fig. 4** *Comparison between the proposed composite controller and the PI controller when* $C_b = 20\,\mu\text{F}$

***(a)*** Reference tracking: PV voltage response with $\tau = 0.001$, ***(b)*** Reference tracking: PV voltage response with $\tau = 0.0008$, ***(c)*** Step response: PV voltage response with $\tau = 0.00025$, ***(d)*** Step response: duty cycle with $\tau = 0.00025$

has proved to be effective regarding disturbance estimation. Indeed, the disturbance $b_2$ coincides with the inductor current $i_L$, which is equal to the PV current $i_p$ in the steady-state regime. The disturbance $b_1$ depends on many factors including the sampling and the switching frequency, the PWM offset, the model uncertainty and other factors that are not considered in the simulation such as the measurement errors.

### *5.3 Tracking performance under model uncertainty*

To further test the robustness of the composite controller consisting of the FBL and the DO, the capacitor $C_b$ and the inductor $L_b$ were incorrectly set in the controller. Moreover, the tracking performance was evaluated for different operating points to test the proposed controller for the whole operating range. For downward steps of PV voltage, $C_b$ and $L_b$ were, respectively, set to be equal to 50 and 150% of their nominal values, whereas, for upward steps, $C_b$ and $L_b$ were, respectively, chosen to be equal to 150 and 50% of their nominal values. Fig. 6 presents the results that correspond to the variation of the capacitor $C_b$, while Fig. 7 illustrates the robustness of the composite controller against the variation of the inductor $L_b$. As can be seen from Fig. 6, the PV output voltage converges in a relatively short time to its new steady-state condition with zero steady-state error, which implies that the observer reacts satisfactory to cancel the error caused by the model uncertainty and the unknown disturbance. More interestingly, the estimate $b_2$ closely follows the inductor current $i_L$ with less fluctuation, indicating that the estimate $b_2$ can replace the current $i_L$ in designing MPPT algorithms with the aim of reducing the measurement noise. On the other hand, Fig. 7 shows that the PV output voltage is robust against the changes in the inductor $L_b$ which confirms the ability of the DO to compensate for the model uncertainties. It is worth mentioning that the fluctuation of the PV voltage is mainly related to the switching frequency and the observer gain that may magnify the measurement noises, particularly when the observer gain is relatively very high.

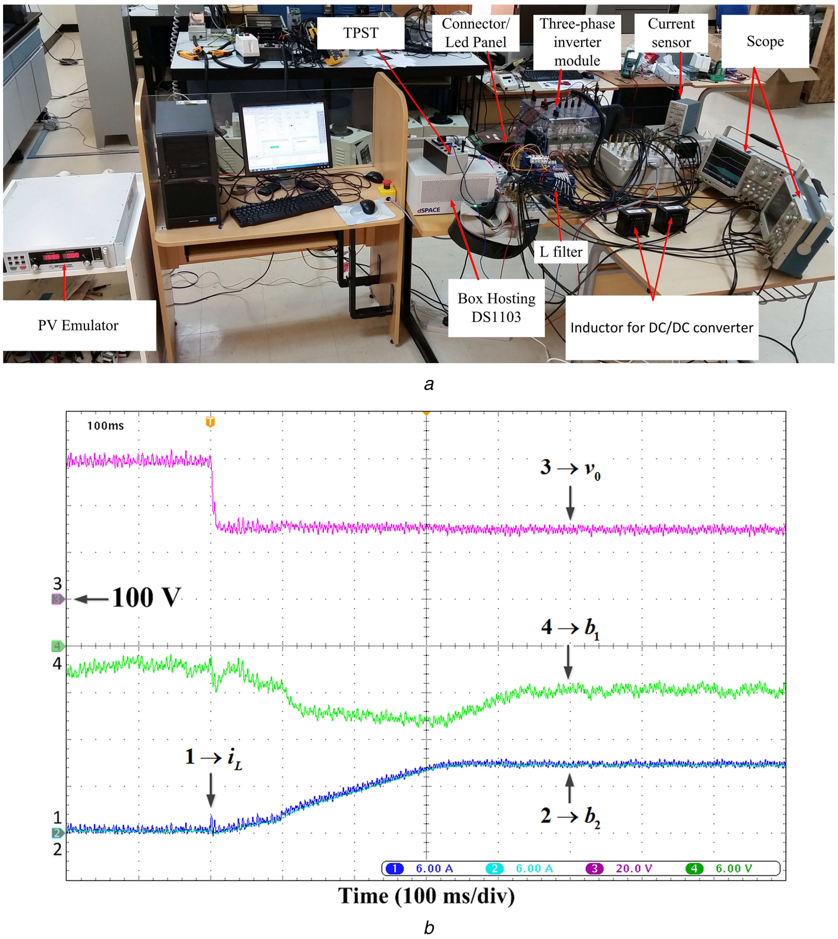


**Fig. 5** *Laboratory setup and experimental results*

***(a)*** Laboratory setup, ***(b)*** PV output voltage, the inductor current and the disturbance with nominal parameters, with $i_L$ (6 A/div), $v_0$ (20 V/div), $b_1$ (6 V/div) and $b_2$ (6 A/div)

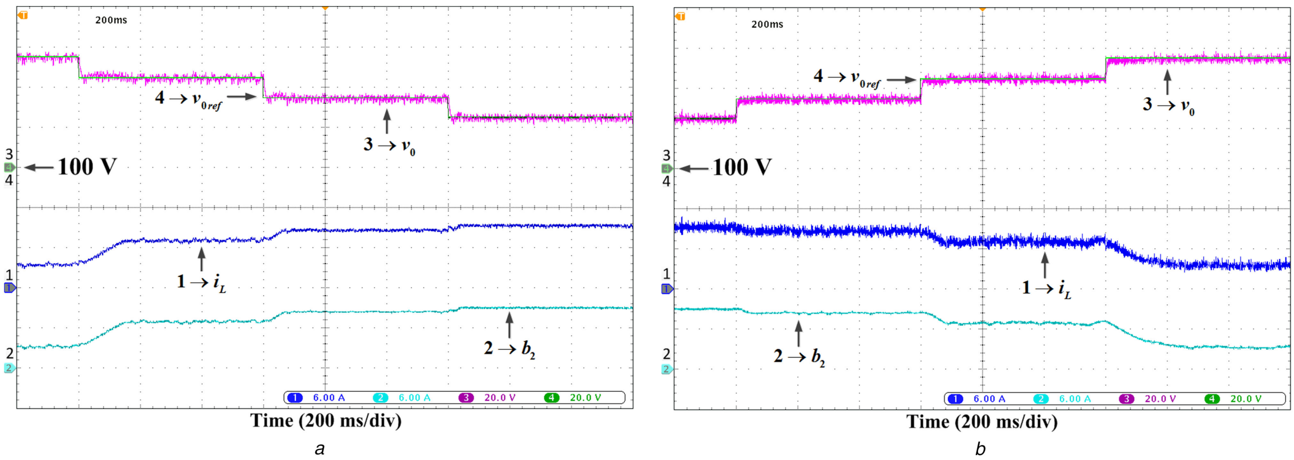


**Fig. 6** *Robustness against $C_b$ variation: the PV output voltage, the inductor current and the disturbance, with $i_L$ (6 A/div), $v_0$ (20 V/div), $b_1$ (6 V/div) and $b_2$ (6 A/div)*

***(a)*** Robustness against $C_b$ variation under downward steps of PV voltage as $v_{0\text{ref}}$: 155 → 145 → 135 → 125 V with $C_b$ is equal to 50% of its nominal value, ***(b)*** Robustness against $C_b$ variation under upward steps of PV voltage as $v_{0\text{ref}}$: 125 → 135 → 145 → 155 V with $C_b$ is equal to 150% of its nominal value

Thereby, it is evident that the PV voltage ripples can be reduced by decreasing the observer gain.

### *5.4 Tracking performance under MPPT algorithm and changes in the solar irradiation*

This experiment was conducted to show the ability of the composite controller to provide a good tracking performance when using an MPPT algorithm. The perturb and observe MPPT algorithm with a variable step size was adopted to extract the maximum power when the solar irradiation changes. The required power for the MPPT algorithm was determined through the use of the estimate $b_2$ instead of the current measurement, and the corresponding results are depicted in Fig. 8. This test was started with a constant solar irradiation of $S = 500\,\text{Wm}^{-2}$ and a constant PV voltage reference of $v_{0\text{ref}} = 155$ V that is approximately equal to the open-circuit voltage associated with $S = 500\,\text{Wm}^{-2}$. This explains why the current $i_L$ is equal to zero during the starting period, i.e. before the time instant $t_0$, at which the solar irradiation was stepped up from 500 to 1000 $\text{Wm}^{-2}$. The MPPT algorithm was enabled just after applying this step increase in the solar irradiation. To further demonstrate the tracking capability of the proposed controller, the solar irradiation was stepped down from 1000 to

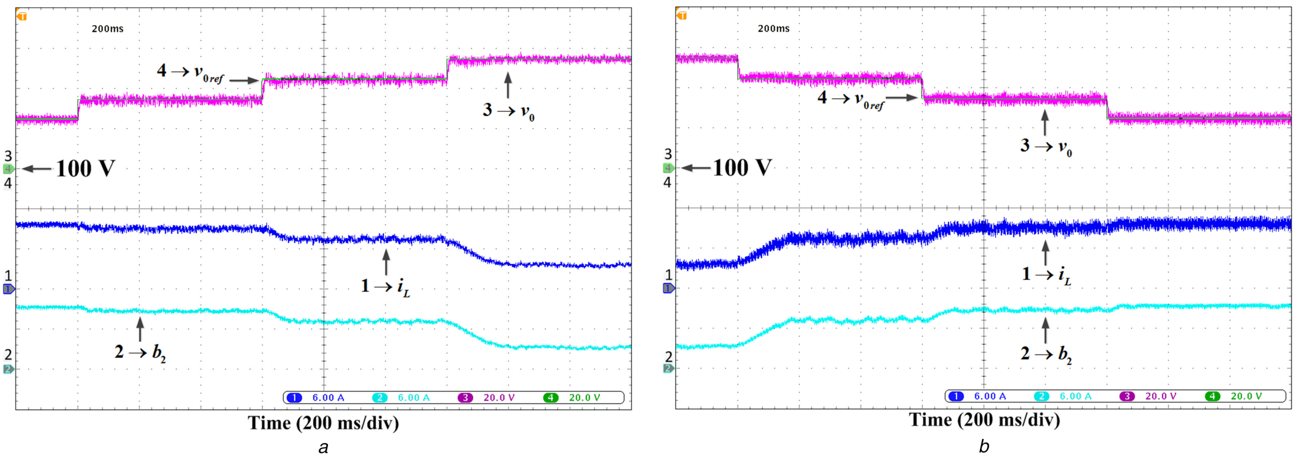


**Fig. 7** *Robustness against $L_b$ variation: the PV output voltage, the inductor current and the disturbance, with $i_L$ (6 A/div), $v_0$ (20 V/div), $b_1$ (6 V/div) and $b_2$ (6 A/div)*

***(a)*** Robustness against $L_b$ variation under upward steps of PV voltage as $v_{0\text{ref}}$: 125 → 135 → 145 → 155 V with $L_b$ is equal to 50% of its nominal value, ***(b)*** Robustness against $L_b$ variation under downward steps of PV voltage as $v_{0\text{ref}}$: 155 → 145 → 135 → 125 V with $L_b$ is equal to 150% of its nominal value

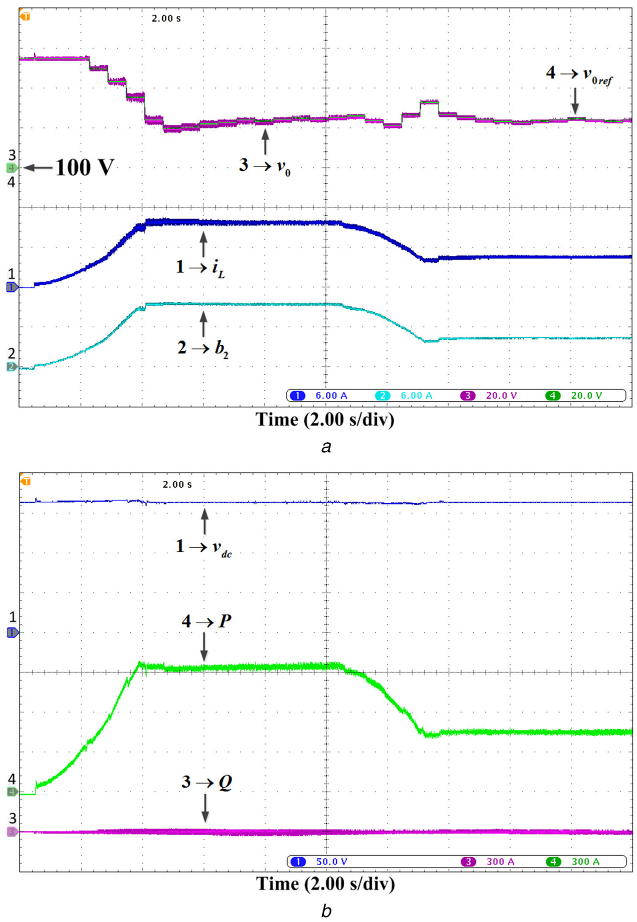


**Fig. 8** *Experimental results illustrating the tracking capability of the composite controller under an MPPT algorithm and a step change of the solar irradiation as $S$: 500 → 1000 → 500Wm$^{-2}$, with $i_L$ (6 A/div), $v_0$ (20 V/div), $b_1$ (6 V/div), $b_2$ (6 A/div), P (300 W/div), Q (300 var/div) and $v_{dc}$ (50 V/div)*

***(a)*** System's response: the PV output voltage, the inductor current and the disturbance under step changes in the solar irradiation and an MPPT algorithm, ***(b)*** dc-link voltage and the active and reactive powers ($P$,$Q$) under step changes in the solar irradiation and an MPPT algorithm with $P$ (300 W/div) and $Q$ (300 var/div)

500 Wm$^{-2}$ at $t = t_1$. As shown in Fig. 8, the PV voltage response exhibits a good tracking performance with zero steady-state error and without any overshoot. The MPPT technique allowed operating around the MPP at the steady-state regime despite the changes in the solar irradiation. It should be noted that the system cannot be experimentally tested under a sudden step change in the inverter power because of the inherent dynamics of the PV emulator in response to a step change in either the solar irradiation or the temperature. The PV emulator limitation also dictated the lower limit of the time step for the MPPT algorithm which was set equal to 0.3 s. It is also worth mentioning that the MPPT performance can be further improved by appropriately designing an advanced MPPT algorithm which is beyond the scope of this paper, as the main focus of this work is the control design for the dc–dc converter and its real-time implementation.

## 6 Conclusion

This paper has described the application of FBL technique to a dc–dc boost converter feeding a grid-connected PV system. A DOBC has been designed and combined with a feedback controller to achieve a zero steady-state error under model uncertainty and external disturbance. The observer adequately captures the unknown disturbances and compensates them in the control law to improve the transient and the steady-state performances. The stability of the closed-loop system under the composite controller has been comprehensively investigated, and it has been proven that the system output tracks its reference with zero steady-state error. Both simulation and experimental results have shown the effectiveness of the proposed controller, and excellent transient and steady-state performances were achieved.

## 7 References

[1] Konstantopoulos, G., Alexandridis, A.: 'Non-linear voltage regulator design for DC/DC boost converters used in photovoltaic applications: analysis and experimental results', *IET Renew. Power Gener.*, 2013, **7**, (3), pp. 296–308

[2] Tang, Y., Bai, Y., Kan, J., *et al.*: 'Improved dual boost inverter with half cycle modulation', *IEEE Trans. Power Electron.*, 2017, **32**, (10), pp. 7543–7552

[3] Tang, Y., Xu, F., Bai, Y., *et al.*: 'Comparative analysis of two modulation strategies for an active buck–boost inverter', *IEEE Trans. Power Electron.*, 2016, **31**, (11), pp. 7963–7971

[4] Tang, Y., Dong, X., He, Y.: 'Active buck–boost inverter', *IEEE Trans. Ind. Electron.*, 2014, **61**, (9), pp. 4691–4697

[5] Tang, Y., Xie, S.: 'System design of series z-source inverter with feedforward and space vector pulse-width modulation control strategy', *IET Power Electron.*, 2014, **7**, (3), pp. 736–744

[6] Subudhi, B., Pradhan, R.: 'A comparative study on maximum power point tracking techniques for photovoltaic power systems', *IEEE Trans. Sust. Energy*, 2013, **4**, (1), pp. 89–98

[7] Renaudineau, H., Donatantonio, F., Fontchastagner, J., *et al.*: 'A PSO-based global MPPT technique for distributed PV power generation', *IEEE Trans. Ind. Electron.*, 2015, **62**, (2), pp. 1047–1058

[8] Lin, F.J., Lu, K.C., Ke, T.H., *et al.*: 'Reactive power control of three–phase grid–connected PV system during grid faults using Takagi–Sugeno–Kang probabilistic fuzzy neural network control', *IEEE Trans. Ind. Electron.*, 2015, **62**, (9), pp. 5516–5528

[9] Kakosimos, P.E., Kladas, A.G., Manias, S.N.: 'Fast photovoltaic-system voltage-or current-oriented MPPT employing a predictive digital current-controlled converter', *IEEE Trans. Ind. Electron.*, 2013, **60**, (12), pp. 5673–5685

[10] Kim, I.-S., Kim, M.-B., Youn, M.-J.: 'New maximum power point tracker using sliding-mode observer for estimation of solar array current in the grid-connected photovoltaic system', *IEEE Trans. Ind. Electron.*, 2006, **53**, (4), pp. 1027–1035

[11] Bianconi, E., Calvente, J., Giral, R., *et al.*: 'A fast current-based MPPT technique employing sliding mode control', *IEEE Trans. Ind. Electron.*, 2013, **60**, (3), pp. 1168–1178

[12] Goncalves Wanzeller, M., Alves, R., da Fonseca Neto, J., *et al.*: 'Current control loop for tracking of maximum power point supplied for photovoltaic array', *IEEE Trans. Instrum. Meas.*, 2004, **53**, (4), pp. 1304–1310

[13] Urtasun, A., Sanchis, P., Marroyo, L.: 'Adaptive voltage control of the DC/DC boost stage in PV converters with small input capacitor', *IEEE Trans. Power Electron.*, 2013, **28**, (11), pp. 5038–5048

[14] Peter, P., Agarwal, V.: 'On the input resistance of a reconfigurable switched capacitor DC-DC converter-based maximum power point tracker of a photovoltaic source', *IEEE Trans. Power Electron.*, 2012, **27**, (12), pp. 4880–4893

[15] Thongpron, J., Kirtikara, K., Jivacate, C.: 'A method for the determination of dynamic resistance of photovoltaic modules under illumination', *Sol. Energy Mater. Sol. Cells*, 2006, **90**, (18), pp. 3078–3084

[16] Nousiainen, L., Puukko, J., Mäki, A., *et al.*: 'Photovoltaic generator as an input source for power electronic converters', *IEEE Trans. Power Electron.*, 2013, **28**, (6), pp. 3028–3038

[17] Xiao, W., Dunford, W., Palmer, P., *et al.*: 'Regulation of photovoltaic voltage', *IEEE Trans. Ind. Electron.*, 2007, **54**, (3), pp. 1365–1374

[18] Freidovich, L.B., Khalil, H.K.: 'Performance recovery of feedback-linearization-based designs', *IEEE Trans Autom. Control*, 2008, **53**, (10), pp. 2324–2334

[19] Chen, W.H., Yang, J., Guo, L., *et al.*: 'Disturbance-observer-based control and related methods–an overview', *IEEE Trans. Ind. Electron.*, 2016, **63**, (2), pp. 1083–1095

[20] Kim, S.K., Choi, D.K., Lee, K.B., *et al.*: 'Offset-free model predictive control for the power control of three-phase ac/dc converters', *IEEE Trans. Ind. Electron.*, 2015, **62**, (11), pp. 7114–7126

[21] Sitbon, M., Schacham, S., Kuperman, A.: 'Disturbance observer-based voltage regulation of current-mode-boost-converter-interfaced photovoltaic generator', *IEEE Trans. Ind. Electron.*, 2015, **62**, (9), pp. 5776–5785

[22] Errouissi, R., Al-Durra, A., Muyeen, S.M.: 'A robust continuous-time MPC of a DC–DC boost converter interfaced with a grid-connected photovoltaic system', *IEEE J. Photovoltaics*, 2016, **6**, (6), pp. 1619–1629

[23] Errouissi, R., Ouhrouche, M., Chen, W.H., *et al.*: 'Robust cascaded nonlinear predictive control of a permanent magnet synchronous motor with antiwindup compensator', *IEEE Trans. Ind. Electron.*, 2012, **59**, (8), pp. 3078–3088

[24] Khalil, H.K.: '*Nonlinear systems*' (Prentice Hall, Upper Saddle River, 2002), vol. 3

[25] Chen, C.C., Lin, Y.F.: 'Application of feedback linearisation to the tracking and almost disturbance decoupling control of multi-input multi-output nonlinear system', *IEE Proc. Control Theory Appl.*, 2006, **153**, (3), pp. 331–341

[26] Khalil, H.K.: '*Nonlinear control*' (Prentice Hall, 2014)

[27] Espinoza-Trejo, D.R., Bárcenas-Bárcenas, E., Campos-Delgado, D.U., *et al.*: 'Voltage–oriented input–output linearization controller as maximum power point tracking technique for photovoltaic systems', *IEEE Trans. Ind. Electron.*, 2015, **62**, (6), pp. 3499–3507

[28] Son, Y.I., Kim, I.H., Choi, D.S., *et al.*: 'Robust cascade control of electric motor drives using dual reduced-order PI observer', *IEEE Trans. Ind. Electron.*, 2015, **62**, (6), pp. 3672–3682

[29] Atassi, A.N., Khalil, H.K.: 'A separation principle for the stabilization of a class of nonlinear systems', *IEEE Trans Autom. Control*, 1999, **44**, (9), pp. 1672–1687

[30] Prasov, A.A., Khalil, H.K.: 'A nonlinear high-gain observer for systems with measurement noise in a feedback control framework', *IEEE Trans Autom. Control*, 2013, **58**, (3), pp. 569–580

[31] Chen, W.-H., Ballance, D.J., Gawthrop, P.J., *et al.*: 'Nonlinear PID predictive controller', *IEE Proc. Control Theory Appl.*, 1999, **146**, (6), pp. 603–611

[32] Errouissi, R., Muyeen, S.M., Al-Durra, A., *et al.*: 'Experimental validation of a robust continuous nonlinear model predictive control based grid-interlinked photovoltaic inverter', *IEEE Trans. Ind. Electron.*, 2016, **63**, (7), pp. 4495–4505

[33] Villalva, M., Gazoli, J., Filho, E.: 'Comprehensive approach to modeling and simulation of photovoltaic arrays', *IEEE Trans. Power Electron.*, 2009, **24**, (5), pp. 1198–1208


# 8 Appendix

### Appendix 1: Dynamic resistance and small-signal modelling

Following [13], the dynamic resistance $R_{\text{pv}}$ is given by

$$R_{\text{pv}} = -\frac{\partial v_0}{\partial i_p} \tag{29}$$

and the current to voltage transfer function can be found by applying the small-signal analysis, yielding

$$H_{cv} = \frac{\tilde{v}_0}{\tilde{i}_p} = \frac{R_{\text{pv}}}{C_b R_{\text{pv}} s + 1} \tag{30}$$

where $\tilde{v}_0$ and $\tilde{i}_p$ are the small-signal values of the state variables $v_0$ and $i_p$, that is

$$v_0 = V_0 + \tilde{v}_0; i_p = I_p + \tilde{i}_p \tag{31}$$

where $V_0$ and $I_p$ are the steady-state values of $v_0$ and $i_p$, respectively. It is clear that the current to voltage transfer function $H_{cv}$ can be approximated with $1/C_b s$ if and only if the condition

$$C_p R_{\text{pv}} \omega_{\text{c}} \gg 1 \tag{32}$$

is satisfied for all $R_{\text{pv}}$, with $\omega_{\text{c}}$ is the angular cutoff frequency of the voltage control. In this study, $R_{\text{pv}}$ falls in the range of [2, 1654] Ω.

### 8.1 Appendix 2: Parameters for simulation and experimental validation

See Tables 1 and 2.

**Table 1** Parameters of the grid-interlinked PV inverter

| | |
|---|---|
| dc link voltage $v_{\text{dc}}$ and $v_{\text{dcref}}$, V | 165 |
| line-to-line grid voltage, V | 86 |
| inverter inductance, mH | 6.8 |
| dc link capacitor, mF | 1.052 |
| frequency, Hz | 50 |
| sampling frequency for the controller, kHz | 10 |
| switching frequency, kHz | 10 |

**Table 2** Parameters for the control of the dc–dc boost converter including the parameters of the cascaded PI controller

| | |
|---|---|
| maximum power of PV unit, W | 1200 |
| boost inductance, mH | 5 |
| input capacitor, mF | 0.16 |
| sampling frequency for the controller, kHz | 10 |
| switching frequency $f_{\text{sw}}$, kHz | 10 |
| the parameter $\tau$ | 0.001 |
| observer gains $(\mu_1, \mu_2)$ | (2, 0.1) |
| natural angular frequency $\omega_{\text{n}i}$, rad/s | 6285 |
| natural angular frequency $\omega_{\text{n}v}$, rad/s | 698 |
| damping ratios $\xi_i$ and $\xi_v$ | 0.7 |